Devil's Staircase–Type Faceting of a Cubic Lyotropic Liquid Crystal

Pawel Pieranski, Paul Sotta, Daniel Rohe, and Marianne Imperor-Clerc

Laboratoire de Physique des Solides, Associé au CNRS, Bâtiment 510, Université Paris-Sud, 91405, Orsay Cedex, France

(Received 17 September 1999)

The faceting of monocrystals of the lyotropic cubic liquid crystals in equilibrium with a humid atmosphere is observed. Experiments reveal the presence of more than 60 different types of facets on the surface of a spherical crystal of radius $R = 1$ mm. The devil's staircase type of faceting has been predicted theoretically when the interaction between steps on the crystal surface is repulsive.

PACS numbers: 61.30.–v, 64.70.Md, 82.65.Dp

One of the most fascinating theoretical aspects of crystal faceting is the "devil's staircase" phenomenon, i.e., the appearance of facets with arbitrarily high Miller indices [1–4]. Experimentally, in all systems investigated to date, such as, for example, metals (Pb [5] or Au [6]), helium [7], or blue phase crystals [8], only a few facets with low Miller indices have been observed. In the case of the lyotropic cubic crystals, the faceting of air bubbles included in large monocrystals was described [9]. Considered as "negative crystals," such bubbles have shown only one family of facets of the {211} type.

Here, we report on the shape of dropletlike lyotropic monocrystals in equilibrium with water vapor of controlled pressure. We show that, unlike the air bubbles, such dropletlike crystals display a surprisingly large variety of facets suggesting a devil's staircase–type mechanism of faceting. We interpret this result as being due to the coincidence of quite large surface tension and reticular distance with an exceptionally low elastic modulus.

The experimental setup is depicted schematically in Fig. 1. Its main part is a tight cell, developed for studying free standing films of lyotropic liquid crystals, in which the humidity h (defined as the ratio of the partial pressure of water vapor to its saturating pressure) is controlled with an accuracy of 0.1% between 0 and 100%. The principle of the humidity control is the same as that used previously in studies of anchoring transitions [10]: two fluxes of nitrogen (or helium), one dry (Φ_d) and the other one saturated with water vapor (Φ_w), are regulated using gas flow controllers, mixed in variable proportions and injected at a typical rate of 100 ml/min into the cell. The temperature of both fluxes and of the cell is regulated between room temperature and 100 °C. Glass windows allow observation with a microscope.

Experiments were performed in the cubic phase of the binary mixture of the nonionic surfactant $C_{12}EO_6$ (hexaethyleneglycol mono n-dodecyl ether) with water [11]. This system has been extensively studied in the past [12], and its phase diagram temperature vs concentration is well known. In particular, it has been well established that the direct cubic phase V_1, present at surfactant concentration between 64.3 and 70.2 wt % at $T = 20$ °C, has the $Ia3d$ symmetry (space group Q_{230}) and can be represented as two identical bicontinuous interwoven surfactant labyrinths separated by a water layer described by the Schoen's gyroid infinite periodic minimal surface [13]. The size of the cubic unit cell is 118 Å. The cubic phase in this system is known for its ability to grow easily very large monocrystals [14].

A small drop of the pure surfactant is deposited on a glass cover slide which is treated with an antiwetting solution in order to obtain a drop with a large range of surface directions. In practice, the surfactant drop spreads a little on the glass surface and forms a spherical cup whose diameter and contact angle at the base are $D \approx 1$ mm and $\theta \approx 30°$, respectively (see Fig. 1). Accordingly, the radius of curvature R of the drop is about 1 mm. In the humid atmosphere of the cell, the drop absorbs water until an equilibrium between the solution and the water vapor is reached. The complete T vs h phase diagram of the $C_{12}EO_6$/water system will be reported elsewhere. It is sufficient to indicate here that the phase sequence is L_2-85%-L_α-95%-V_1-98%-H_1-100%-L_2 at $T = 20$ °C. Thus, the transition from the L_2 (inverted micellar) phase to the L_α (lamellar) phase takes place at $h = 85\%$ (without any metastability, since the lamellar phase wets the micellar phase) and the drop usually keeps approximately its spherical shape. The transition from the lamellar to the cubic phase V_1 is significantly metastable and occurs

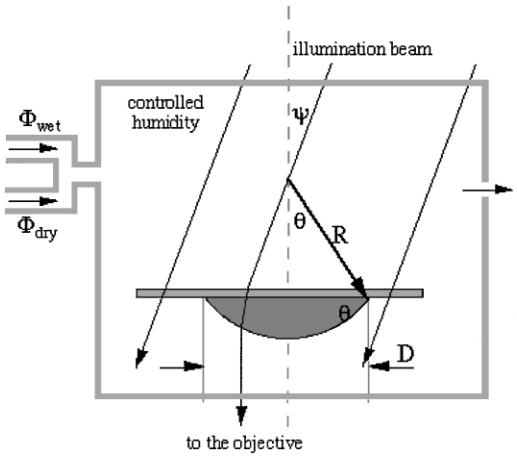

FIG. 1. Experimental setup.

for supersaturations $\Delta h \approx 1\%$. One observes a rapid dendritic growth of the cubic phase nucleated on dust particles. Whenever the transition starts from one germ only, a monocrystal fills the drop. Immediately after the phase transition, the surface of the drop is very irregular. After 1 h annealing at constant T and h, the drop surface gets smoother and facets start to appear on it. One or two days of annealing are necessary to obtain the faceting shown in Figs. 2 and Fig. 3. In these photographs, facets coexist with rough parts of the crystal surface. These constellations of facets stay stable as long as temperature and humidity are maintained constant.

The images were obtained in transmission mode. The best contrast between facets and rough parts of the crystal surface was achieved with the microscope set slightly out of focus and with illumination by a slightly diverging light beam making an angle ψ with the optical axis (Fig. 1). In these conditions, only a small portion of the drop surface appears as illuminated because a low aperture objective ($\times 5, \mathrm{NA} = 0.13$) was used for observation.

The most striking feature of the photographs (Figs. 2 and 3) is an astonishing variety of facets with different Miller indices. All these facets form a highly symmetric pattern very similar to Laue diagrams. In order to identify the Miller indices of all facets, a polar diagram in which the positions of all $[hkl]$ directions with $h, k, l = 0, \ldots, 12$ are indicated by circles on a sphere was used (Fig. 4). Figure 4 shows one elementary patch. The whole crystal habit is composed of 48 identical elementary patches, related by the symmetry O_h of the cubic crystal. It is thus sufficient to index one elementary patch as shown in Fig. 4. In this heuristic diagram, the diameters of circles have been set proportional to $d_{hkl} = a/(h^2 + k^2 + l^2)^{1/2}$, since the occurrence and relative extension of facets is directly related to the interplanar distances d_{hkl} according to the elementary Donnay-Harker theory [15]. For the same reason, the general crystallographic selection rules for the $Ia3d$ symmetry were applied, so that only those facets were drawn for which the four following relations are satisfied. (a) hkl: $h + k + l = 2n$; (b) $hk0$: $h, k = 2n$; (c) hhl: $2h + l = 4n$; (d) $h00$: $h = 4n$, where n is an integer. Finally, the circles were drawn as black or white when the sum $h^2 + k^2 + l^2$ is smaller or larger than 170, respectively. The choice of this cutoff value is empirical and results from our observations.

The observed facets were identified by comparing photographs with corresponding portions of the elementary patch (Figs. 2 and 3) and measuring the slopes of several facets by interferometry [16]. As a result, about 60 facets with different Miller indices have been identified. The relative sizes of observed facets correspond roughly to the model based on the reticular distances d_{hkl} only. Nevertheless, there are some clear discrepancies. For example, according to this model, the (321) facet should be larger than the (431) one, whereas the inverse obviously occurs in Fig. 2b. In fact, this discrepancy is not surprising: besides the interreticular spacing d_{hkl}, the Donnay-Harker-type models involve an effective potential

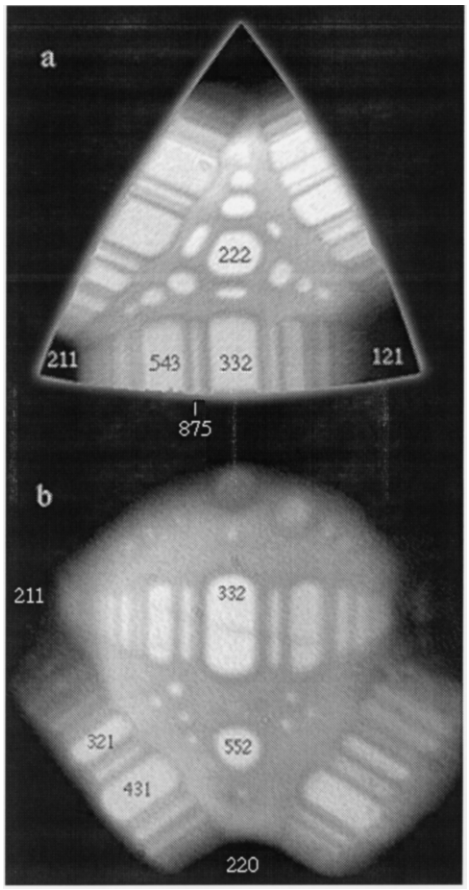

FIG. 2. Views of a faceted monocrystal: (a) in the vicinity of the (222) facet; (b) in the area between (220), (211), and (121) facets. Note the presence of tracks, made of facets with parallel edges, connecting the (211) and (121) facets in (a) and the (211) and (220) facets in (b).

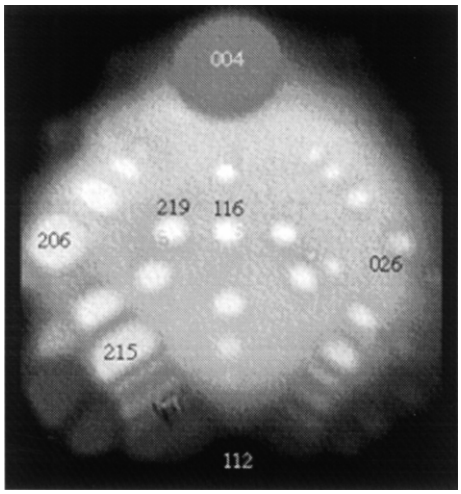

FIG. 3. View of a faceted monocrystal in the area between the (004) and (112) facets. Note that the sizes of the (206) and (026) facets are different.

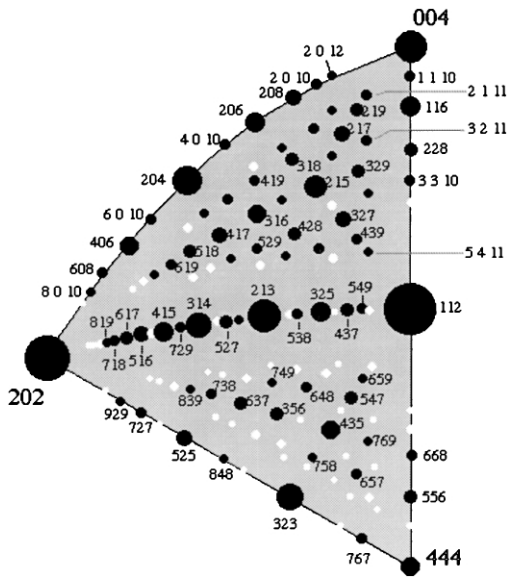

FIG. 4. Theoretical scheme with Miller indices of facets observed experimentally.

of periodicity d_{hkl} which fixes the minima of the surface energy at discrete levels separated by the distance d_{hkl} [17]. In lyotropic cubic crystals, the depth of these minima must be related to the distribution $\rho(\mathbf{r})$ of the surfactant inside the crystal or more precisely to the amplitude ρ_{hkl} of its Fourier component in the direction $[hkl]$. This last quantity is the structure factor which is directly measured in x-ray diffraction experiments. In the case considered here of the (321) and (431) facets, it is remarkable that the 431 Bragg peak has been found much more intense than the 321 one, both in the $C_{12}EO_6$/water mixture [12] and in other lyotropic systems with the same cubic structure [18], as well as in theoretical computations of the structure factor of a gyroid infinite periodic minimal surface decorated with a film of water [19].

Another remarkable feature of the observed faceting pattern is the presence of "tracks" in which many facets with parallel edges and different widths are packed. Two different types of tracks are observed easily: one connecting different {211} facets [see Fig. 2(a)], and the other one connecting {211} to {220} facets [see Fig. 2(b)]. Obviously, 2D devil's staircase models of faceting, based on the interaction between parallel steps, come to mind. If the vectors $\mathbf{a} = [2, 1, 1]/6$ and $\mathbf{b} = [1, 2, 1]/6$ are taken as a basis $[\mathbf{a}, \mathbf{b}]$ of a 2D crystal (a section of the 3D crystal by a plane containing the track), then all (hkl) facets on the (211)-(121) track can be indexed as (mn) facets in this 2D basis according to

$$(hkl) = m(211) + n(121). \tag{1}$$

For example, the (332) facet in the middle of the track corresponds to the (11) facet in the 2D crystal, the (543) facet to (21), (754) to (31), (965) to (41), or (875) to (32), etc. As shown for the first time by Landau [20], at $T = 0$ any (mn) facet can be created by an appropriate periodic arrangement of steps commensurate with the crystal lattice, and made stable by a repulsive interaction between steps. At $T = 0$, the only limit for realizing an (mn) facet is geometrical and is due to the finite size R of the crystal. According to Schulz [1], for a repulsive potential $U \sim p^{-\delta}$, where $p = m/n$ is the average distance between steps (in units of d_{211}), the width of the (mn) facet on the crystal surface is of the order of $Rp^{-\delta-1}$. This width obviously cannot be smaller than the distance between two steps, which is pd, so that one gets

$$p_{\max} = \left(\frac{R}{d}\right)^{1/\delta+2}. \tag{2}$$

As shown by Marchenko and Parshin [21], the potential energy of the elastic interaction per unit length between two steps at a distance $x = pd$ on a crystal surface is given by the $\delta = 2$ law:

$$U(p) = \frac{2(1-\sigma^2)\gamma^2}{\pi E}\,\frac{1}{p^2}, \tag{3}$$

where γ is the surface tension of the crystal surface on which steps appear, E is the Hook modulus, and σ the Poisson ratio of the crystal. As a consequence of this $\delta = 2$ law, for $R = 0.1$ cm and $d = 5 \times 10^{-7}$ cm, $p_{\max}$ must be less than 30. Let's notice that in the tracks visible in Fig. 2, parallel edges of facets have roughly the same length. This feature has been predicted at $T = 0$ by Burkov [3] within a model of a simple cubic crystal with atoms interacting via a $r^{-\gamma}$ potential (with $\gamma > 4$).

At $T \neq 0$, this theoretical limit for p cannot be reached because thermal fluctuations of steps on facets with large Miller indices make them rough. These fluctuations imply the presence of kinks on steps, so that the third dimension must be taken into account and the (mn) facet of the 2D model must be seen as the $(mn0)$ facet in a 3D model. The amplitude of fluctuations depends on the strength of the elastic repulsion between steps. On the $(mn0)$ facet, where the average distance between steps is pd, Eq. (3) gives a typical energy per unit length γ^2/E, so that $\gamma^2 d/E$ is the energy that has to be compared with kT. According to Schulz [1], the roughening temperature T_c for the $(mn0)$ facet is given by

$$kT_c e^{E_0/kT_c} = \frac{1}{4}\,\frac{d^2U(p)}{dp^2}\,pd, \tag{4}$$

where E_0 is the energy of a kink, which gives, if E_0 is small compared to kT,

$$kT_c \approx \frac{\gamma^2 d}{E}\,\frac{1}{p^3}. \tag{5}$$

As expected, the energy $\gamma^2 d/E$ is the pertinent thermodynamic quantity that has to be considered at finite T. The surface tension $\gamma \approx 25$ dyn/cm of the {211} crystal surface has been estimated from the frequency of vibration of free-standing films [16]. The shear elastic modulus $E \approx 10^7$ erg/cm^3 has been estimated from the frequency of vibration of the bulk cubic phase contained in a cylindrical test tube [22]. When compared to other systems,

cubic lyotropic liquid crystals appear now to be exceptional because a quite large value of the surface tension coincides with a relatively low elastic modulus. As a consequence, the characteristic energy $\gamma^2 d/E$ is of the order of 3×10^{-11} erg. This is much larger than the thermal energy kT ($\approx 10^{-14}$ erg at 300 K). Thus, the maximum p value estimated from Eq. (5) is $p_{\max}(300\ \mathrm{K}) \approx 14$. Although very crude, this argument may explain why so many facets with different Miller indices occur here.

Note that in blue phase I monocrystals, the crystallite size R was about 200 μm and the interplanar distance d about 0.2 μm, so that from Eq. (2) one gets $p_{\max}$ of the order of 5. In other words, on such small crystals with so high steps, there is simply no space for forming facets with large Miller indices. The case of the faceted air bubbles seems more puzzling. The most important difference between the droplets considered here and the air bubbles is their long term stability. The pressure must be larger inside a bubble of radius R than outside the crystal by the amount $\Delta p = \gamma/R$. Since the cubic phase is not completely impermeable to the gas, the bubble will deflate due to diffusion of the gas through the crystal. As a consequence, the observed bubble shapes may not correspond to the equilibrium state.

In the present case, the observed shapes are certainly not at equilibrium either. Indeed, some facets from the same $\{hkl\}$ family do not have the same extension on the whole monocrystal, even after annealing a few days at constant T and h. For example, in Fig. 3, the (206) facet is larger than the equivalent (026) one. Moreover, the relative surface areas of facets and rough parts depend on humidity; after a small increase in humidity, all facets expand until rough parts shrink to a system of edges and vertices. A further increase in humidity results in the expansion of principal facets (with small Miller indices, such as {211} or {220}) and the corresponding disappearance of facets with larger Miller indices. Both effects are similar to a crystal growth process in which new atoms are added first to rough parts of the crystal surface and, subsequently, to the steps and kinks forming vicinal facets. In the present case, these processes must be understood as being due to an increase of the number of cubic unit cells contained in the drop. When the cubic crystal forms, surfactant molecules are distributed in unit cells. If the number of surfactant molecules per unit cell n_s depends on the humidity h, then a change in humidity must result in a change of the number of unit cells in the crystal since the total amount of surfactant is fixed. If n_s decreases, new unit cells must be created. The most appropriate locations for these new unit cells are edges of the crystal facets, so that facets should expand. Thus, the observed effect may reflect a decrease of the number n_s of surfactant molecules per unit cell upon hydration of the crystal.

In conclusion, we have reported here the first observation of a devil's staircase–type faceting predicted theoretically in the framework of models describing vicinal facets as periodic systems of steps interacting via an elastic repulsion. We have pointed out that this interaction is much larger in cubic lyotropic liquid crystals than in other systems because large surface tension and unit cell dimension coincide with a small elastic modulus. For this reason, vicinal facets with large Miller indices, on which steps are far apart, do not melt at room temperature.

The experimental device was built by V. Klein with the assistance of B. Ranchin, who are gratefully acknowledged. This work benefited from fruitful discussions with Philippe Nozières and Heinz Schulz.

[1] H. J. Schulz, J. Phys. (Paris) **46**, 257 (1985).
[2] L. A. Bol'shov, V. L. Pokrovski, and G. V. Uimin, J. Stat. Phys. **38**, 191 (1985).
[3] S. E. Burkov, J. Phys. (Paris) **46**, 317 (1985).
[4] C. Rottman and M. Wortis, Phys. Rev. B **29**, 328 (1984).
[5] J. C. Heyraud and J. J. Métois, Surf. Sci. **128**, 334 (1983); C. Rottman, M. Wortis, J. C. Heyraud, and J. J. Métois, Phys. Rev. Lett. **52**, 1009 (1984).
[6] J. C. Heyraud and J. J. Métois, J. Cryst. Growth **50**, 571 (1980); Acta Metall. **28**, 1789 (1980).
[7] P. E. Wolf, S. Balibar, and F. Gallet, Phys. Rev. Lett. **51**, 1366 (1983).
[8] P. Pieranski, R. Barbet-Massin, and P. E. Cladis, Phys. Rev. A **31**, 3912 (1985).
[9] P. Sotta, J. Phys. (Paris) II **1**, 763 (1991).
[10] J. Bechhoefer, J.-L. Duvail, L. Masson, B. Jérôme, R. M. Hornreich, and P. Pieranski, Phys. Rev. Lett. **64**, 1911 (1990).
[11] D. J. Mitchell, G. J. T. Tiddy, L. Waring, T. Bostock, and M. P. McDonald, J. Chem. Soc. Faraday Trans. **79**, 975 (1983).
[12] Y. Rançon and J. Charvolin, J. Phys. (Paris) **48**, 1067 (1987); M. Clerc, P. Laggner, A.-M. Levelut, and G. Rapp, J. Phys. (Paris) II **5**, 901 (1995).
[13] J. Charvolin and J. F. Sadoc, J. Phys. (Paris) **48**, 1559 (1987).
[14] M. Clerc, Y. Hendrikx, and B. Farago, J. Phys. (Paris) II **7**, 1205 (1997).
[15] See, for example, in F. C. Phillips, *An Introduction to Crystallography* (Longmans, New York, 1960).
[16] D. Rohe, B. Ranchin, L. Sittler, and P. Pieranski (unpublished).
[17] P. Nozières (private communication).
[18] V. Luzzati, A. Tardieu, T. Gulik-Krzywicki, E. Rivas, and F. Reiss-Husson, Nature (London) **220**, 485 (1968).
[19] M. Clerc and E. Dubois-Violette, J. Phys. II (Paris) **4**, 275 (1994).
[20] L. D. Landau, *Collected Papers* (Pergamon Press, Oxford, 1971).
[21] V. I. Marchenko and A. I. Parshin, JETP **52**, 129 (1980).
[22] P. Sotta and P. Pieranski (unpublished).